

Robot-based Automated Nanohandling

Thomas Wich and Helge Hülsen

Division of Microrobotics and Control Engineering,
Department of Computing Science,
University of Oldenburg, Germany

2.1 Introduction

Within the last ten years, the interest of industry and research and development institutes in the handling of micro- and nanometer-sized parts has grown rapidly [1]. Micro- and nanohandling has become a very common task in the industrial field and in research in the course of ongoing miniaturization. Typical applications include the manipulation of biological cells under an optical light microscope, the assembly of small gears for miniaturized gearboxes, the handling of lamellae cut out of a silicon wafer in the semiconductor industry, and the chemical and physical characterization of nanoscale objects. The number of applications for nanohandling and nanoassembly is expected to grow rapidly with the development of nanotechnology. The handling process is the precursor of the assembly process, hence, in this chapter, these expressions are used equally where not explicitly stated.

Often, a distinction is made between macro-, micro-, and nanoscale assembly with respect to the part size, where the part dimensions are larger than 1 mm for macroscale, smaller than 1 mm for microscale, and smaller than 1 μm for nanoscale handling [2]. This distinction should even be tightened, because the interaction between the handling system and the handled parts is mostly determined by its smallest dimension, which determines the necessary **positioning accuracy** (Chapter 1). A typical example for parts with very exotic aspect ratios, but which are still considered as nanometer-sized parts, are nanofibers or nanotubes. They can, *e.g.*, be produced by electro-spinning [3], which results in lengths in the cm-range. However, most of these handling processes are still accomplished by means of manual operation [4-6]. Very often, this leads to either very long process durations with high reliability or to shorter durations with low reliability.

The handling process itself can be distinguished by the number of parts handled at a time, *i.e.*, when only one part is handled at a time the expression **serial**

approach is used, in contrast to **parallel approach** for simultaneous handling of multiple parts [2]. These two approaches are based on very different considerations: the serial approach is the more conservative one, where the principles of handling known from the macroscale are adapted to the micro- and nanoscale. Naturally, special considerations have to be taken into account when downscaling, which is one of the main issues discussed in this chapter.

The other approach is the parallel handling of micro- and nanometer-sized parts, where force fields are used to position and orientate objects. The aim here is to maintain the advantages of batch processes, as applied in the MEMS (micro-electro-mechanical systems) and semiconductor industries.

Handling processes can be evaluated in respect of two parameters: **throughput** and **reliability**. (Massively) parallel handling or manufacturing aims at very high throughputs, *e.g.*, assembly of dies in the semiconductor industry. In contrast, the serial approach handles only one part at a time, where high reliability is the main requirement because of the special value of the handled parts. A typical example is the handling of TEM (transmission electron microscope) lamellae that are small slices (approx. $20\text{ }\mu\text{m} \times 10\text{ }\mu\text{m} \times 100\text{ nm}$) cut out of a processed silicon wafer by a focused ion beam (FIB). These lamellae are then transferred to a TEM for inspection, *i.e.*, the TEM lamellae are the micrographs of the semiconductor industry. This approach is very important for discovering failures in semiconductor processes, and high reliability of handling is required. In general, the criteria to be considered when distinguishing between a serial and a parallel approach are the number of parts to be handled or assembled, the complexity of the process, and the individuality of the single parts.

The given examples for the serial and parallel approach represent two applications with very different demands. Still, the goal is always to maximize reliability and throughput for every handling system, independent of the chosen approach, but sometimes reliability is more important than throughput, and vice versa. This chapter focuses on automation issues in the field of **nanohandling for the serial approach**.

The handling of nanoscale objects usually takes place in a special environment necessary for observation, *e.g.*, under optical microscopes or scanning electron microscopes (SEM). The advantages and disadvantages of the single **vision sensors** and resulting consequences for the handling of objects with respect to automation will be discussed in Section 2.2. When the size of the handled objects is reduced, the relationship between surface and volume changes dramatically, resulting in a stronger influence of **parasitic forces** on the objects compared to the macroworld. These forces have to be overcome in order to successfully automate handling and assembly processes (more information in Section 2.3). Another major issue for the process automation discussed in Section 2.3 is the **contact detection**, which is the detection of height distances between objects. Critical issues regarding handling processes and the **planning** of these processes by a combination of simple tasks and subtasks will be discussed in Section 2.4. Based on these, measures and approaches for **optimizing reliability and throughput** of handling and assembly processes will be described and discussed in Section 2.5. The setup and results

achieved with an **automated microrobot-based nanohandling station (AMNS)**, implemented for the handling of TEM lamellae, will be described in Section 2.6.

2.2 Vision Sensors for Nanohandling Automation

Nanohandling can be seen as the continuation of macrorobotics to the nanometer scale, taking several new issues into account. One of these issues is the need for a near-field vision sensor (Chapter 1), providing visual information about the handling process, *i.e.*, making the nanoworld accessible to the human eye.

Although nanohandling tasks could be performed without any visualization by relying on measurement data from the handling tools like forces, velocity, and time, it is much more precise to measure geometric values (position, length, distance, *etc.*) directly using vision-based sensors. As will be shown in Section 2.4, especially for nanohandling tasks the continuous gathering of geometric information is very important to achieve high reliability. There are three main reasons for this:

1. The **parasitic forces** result in an apparently unpredictable behavior of objects, as many parameters for these parasitic forces are either unknown or change continuously. A typical example is the release of a small micro- or nanoscale object from a gripper. Opening the gripper jaws does not necessarily lead to dropping the object due to gravitation; instead the object often sticks to one of the jaws due to parasitic forces.
2. The sensors that are used in nanohandling and manufacturing to determine an object's state (*e.g.*, “gripped”), position (*e.g.*, “distance to the gripper”) or orientation (“upright”) are usually bigger in size than the objects themselves. By contrast, when handling parts in the macroscale, the sensors are smaller or in the same range as the tools. For example, modern grippers can easily handle an egg without damaging it, due to integrated force sensors, whereas the integration of force sensors into a gripper with a jaw cross-section of a few micrometers is extremely challenging (Chapter 6). Thus, on the nanoscale the **sensor density**, *i.e.*, the amount of sensors per handling tool, is much smaller than on the macroscale.
3. The near-field vision sensors (Chapter 1) considered are **global vision sensors**, *i.e.*, they measure a scene based on a global coordinate system.

The combination of the first two circumstances – apparently undetermined behavior of the objects due to hardly determinable parasitic forces and a significantly lower sensor density – are the major challenges for any nanohandling process.

Vision sensors, however, provide a tremendous amount of information, because objects can be recognized and their relationship to each other can thus be qualified and quantified. A typical example is the gripping of a small glass sphere, where it is necessary to know if the sphere is between the gripper jaws. By evaluating this information using object recognition, it is possible, *e.g.*, to operate without a force sensor on the gripper jaws.

2.2.1 Comparison of Vision Sensors for Nanohandling Automation

Of further interest are the **geometric scales**, which have to be bridged during nanohandling tasks. Consider a typical robot used for assembly tasks in the automotive industry. The range of the robot is several meters ($\sim 10^0$ m), and typical position accuracies are in the range of a millimeter ($\sim 10^{-3}$ m); the dimension of the geometric scale is four orders of magnitude. As a comparison, the range of the AMNS described in Section 2.6 is from one decimeter ($\sim 10^{-1}$ m) to a position accuracy of 100 nm ($\sim 10^{-7}$ m), thus seven orders of magnitude are passed through. For most applications, it is preferable to have a vision sensor that can be zoomed seamlessly, in order to cover the full range of geometric scale.

The resolution of the imaging sensor is defined by the distance between two objects needed to recognize them as separated. Therefore, the resolution indicates the size of the object, which the imaging sensor can track in a handling process. However, it must be kept in mind that among other factors, the resolution in the scanning microscopy is strongly dependent on the **image acquisition time**, *e.g.*, the slower an image is scanned, the better the resolution becomes.

The image acquisition time has a major influence on the automation process, not only with respect to the image quality. It also determines the maximum velocity with which objects or tools can be moved under observation. This topic will be discussed in Section 2.2.3.

Of considerable interest for object recognition purposes and for the user is the **information** contained in the image acquired from the sensor. Images based on light from the visible spectrum can be colored (light optical microscope) with the colors giving information about the geometric surface of the object. By contrast, images gathered by an SEM using an energy dispersive X-ray detector (EDX-detector) contain information about the material from a depth of up to 3 μ m from the object's surface. Images gathered by a scanning probe microscope (SPM), *e.g.*, an atomic force microscope (AFM), contain information about the tip-sample interaction, *i.e.*, the distinction between two objects lying on each other is hardly possible without previous knowledge. With regard to automation of handling tasks, the necessary information is based on geometric conditions (*e.g.*, "position", "orientation" and "distance"). However, the information contained in an image can be of different quality, *e.g.*, material, material contrast, conductivity, or atomic forces. Thus the mapping from the image information to the geometric information about an object condition can in many cases only be fulfilled with previous knowledge.

The **interactions** between sensor medium and object have also to be considered as the medium influences the object. For example, in the SEM, the electron beam used for scanning the object can lead to electrical charging of the object or even to damage. The tip of an AFM used for scanning an object can move the object due to parasitic forces and thus accidentally interfere with a handling process.

Very important for handling tasks is the **dimensionality** of the gathered image. Two-dimensional images are common, *e.g.*, in light microscopy or SEM. Necessary for handling tasks is often the determination of the geometric condition

of the object in three dimensions, which has to be done when only 2D images are available. Specialized methods are discussed in Section 2.3.2 and in Chapter 5.

Other issues are the environmental requirements and the constraints imposed by the vision sensor. Typical restrictions are given in installation space, vacuum compatibility, and electromagnetic shielding.

Three typical vision sensors used for nanohandling are given in Table 2.1. The **light microscope** has its major domain as a vision sensor for the handling of micro-sized parts, due to its comparatively low resolution. Still, the frame rate is only determined by the quality of the camera grabbing the images and not by the medium itself, as it is not a scanning vision sensor. Furthermore, the geometric information can be directly evaluated. The 2D images with a low depth of focus are well suited for automation purposes, as the height difference between two objects can easily be quantified (Section 2.3.2).

Within this book the focus regarding vision sensors is on **scanning electron microscopes**, whose major advantages are their high resolution combined with a high range of magnification. The information contained in the images about the objects is mapped to geometric conditions, even with the commonly used Everhart-Thornley SE detector. Further advantages can be drawn from imaging with specialized detectors (*e.g.*, object recognition through material identification). A drawback for automation is certainly the comparatively low frame rate. The consequences of this issue are considered in Section 2.3, and possible solutions are presented in Chapter 4. Additionally, the high depth of focus of the 2D images complicates the determination of height distances between objects. Solutions for this problem will be discussed in Section 2.3.3. The electron beam scanning the objects and tools can also lead to electric charging and thus undetermined parasitic forces.

Atomic force microscopes become more and more interesting for the automation of nanohandling tasks where the object's size is only a few nm. Due to its very high resolution, the AFM – or more generally the SPM – is the only option. However, its very low frame rate prevents the automation of processes at reasonable speeds; this might change when the first high-speed AFMs become commercially available [7]. From an automation aspect, the generation of image information that can easily be transferred into three-dimensional views of the handling process is very advantageous, although a reference level (usually the substrate, on which the objects are placed) has to be present.

Recapitulating the issues discussed above, the conclusion can be drawn that the light microscope has the most advantages regarding microhandling. The low requirements with regard to the environment and the sensor medium make it a comparatively cheap and flexible sensor. Although light microscopes can open the door to the nanometer range, automation of nanohandling is hardly possible due to a lack of geometric information. For example, silicon nanowires with a diameter of a couple of hundred nanometers and a length of several micrometers are visible under the light microscope as interference.

The application of AFMs for nanohandling tasks is reasonable for extremely small objects. The gap between light microscopy and AFM is best bridged using SEMs.

Table 2.1. Comparison of light microscope, SEM, and AFM as vision sensors for nanoscale automation

	Light microscope	Scanning electron microscope (SEM)	Atomic force microscope (AFM)
Resolution	Several hundred nm	1-3 nm for thermionic electron guns, approx. 0.1 nm for field emission guns	$\ll 1$ nm
Orders of magnitude in scale (oom) = difference between field length at least magnification and resolution	$10^{-2} \text{ m} - 10^{-7} \text{ m}$ 6 oom	$10^{-3} \text{ m} - 10^{-10} \text{ m}$ 8 oom	$10^{-4} \text{ m} - 10^{-10} \text{ m}$ 7 oom
Frame rate or image acquisition time	Approx. 25 frames per second, $T = 40$ ms	$T = 0.1 - 100$ s, depending on image quality and size	$T = 10 - 100$ s, 15 ms have been reported for high speed AFMs [7]
Image information	<ul style="list-style-type: none"> •Surface condition •Color •Geometric shape 	<ul style="list-style-type: none"> •Topography (SE detector) •Material contrast (SE/BSE detector) •Material (EDX detector) 	<ul style="list-style-type: none"> •Tip-sample interaction, force, height
Interaction between vision medium and object	Visible light, interactions used for optical trapping	Electron beam, can lead to charging, heating, and damage	Force between AFM tip and object is measured, surface can be damaged, object can interfere with the tip
Image dimension	2D low depth of focus	2D high depth of focus	3D
Environment	Ambient atmosphere	High vacuum or reduced pressure	Ambient atmosphere

2.2.2 Zoom Steps and Finding of Objects

Although the handled objects are in the nanometer to micrometer range, they must often be transported over several centimeters (*e.g.*, handling of TEM lamellae). For assembly applications, micro- to nanometer-sized parts must mostly be joined onto parts with a size of several millimeters (*e.g.*, bonding of carbon nanotubes on AFM tips).

Therefore, several orders of magnitude on the geometric scale have to be gone through, mostly starting on the centimeter scale and zooming in multiple steps. Typical examples for the different zoom steps are given in Figures 2.14 and 2.15. Usually, after every zoom step a positioning step follows, in order to center the object for the next zoom step.

Quite often, different actuators and/or sensors are used for different magnifications, *e.g.*, a DC motor for coarse positioning at low magnifications and a piezo drive for fine positioning at high magnifications. Consequently, every combination of a zoom step and its subsequent positioning step has to be seen as a task of its own in the process chain with its individual reliability (Section 2.4). Hence, the number of **zoom-and-center (ZAC) steps** should be minimized. It is therefore of considerable interest to calculate how many ZAC steps are at least necessary, until an object is sufficiently magnified, starting from a defined imaged area.

For determining the number of steps, the following approach is sensible: the imaged area should be square-shaped with an edge length k_n ; the minimum edge length of the next (k_{n+1}) magnification step can then be determined by the following equation:

$$k_{n+1} = H \cdot s + u_{pos} + \frac{u_{pixel}}{A_{pixel}} \cdot k_n. \quad (2.1)$$

In Figure 2.1, the single terms are illustrated. The term $H \cdot s$ represents the minimum desired image size, consisting of the structural size s of the object and the hull factor H . The structural size s is the size of an object (*e.g.*, diameter of a carbon nanotube, CNT) or the distance between object and tool in a handling process. The hull factor H determines the image size compared to the object size needed for the handling process.

After every zoom step, the object is centered again. The actuator performing this positioning step has an accuracy of u_{pos} , which has to be added to the hull. Furthermore, the edge length k_{n+1} of the $(n+1)$ th zoom step depends on the accuracy of the object recognition of the n -th step, *i.e.*, defining the maximum difference between measured and real position. The term $u_{pixel} \cdot k_n / A_{pixel}$ reflects the object recognition accuracy, consisting of the number of pixels A_{pixel} per edge length k_n and the accuracy of the object recognition u_{pixel} given in pixels.

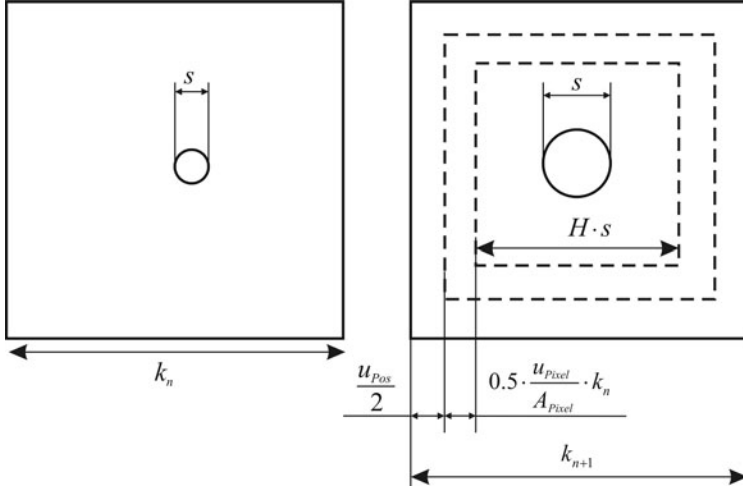


Figure 2.1. Two subsequent zoom-and-center steps during magnification of the object with diameter s . The left image has a lower magnification compared to the right one, *i.e.*, $k_n > k_{n+1}$. In the right image, the parameters used in Equation 2.2 are shown. The inner square is used as the area of movement for the object with a diameter s .

Based upon the above equation, the edge length of the n -th zoom step can be calculated by transferring the recurrence relation in Equation 2.1 into an explicit expression for k_n :

$$k_n = \left(k_0 - \frac{H \cdot s + u_{pos}}{1 - u_{pixel} / A_{pixel}} \right) \cdot \left(\frac{u_{pixel}}{A_{pixel}} \right)^n + \frac{H \cdot s + u_{pos}}{1 - u_{pixel} / A_{pixel}}. \quad (2.2)$$

Assuming that the edge size of the n -th frame should be equal to the ε -tolerated sum of the hull and inaccuracies through positioning and object recognition, Equation 2.2 can be written as

$$(1 + \varepsilon) \cdot (H \cdot s + u_{pos}) \cdot \left(1 + \frac{u_{pixel}}{A_{pixel}} \right) = \left(k_0 - \frac{H \cdot s + u_{pos}}{1 - u_{pixel} / A_{pixel}} \right) \cdot \left(\frac{u_{pixel}}{A_{pixel}} \right)^n + \frac{H \cdot s + u_{pos}}{1 - u_{pixel} / A_{pixel}}. \quad (2.3)$$

Equation 2.3 can then be solved for n , thus returning the minimum number of ZAC steps needed for automated switching from low magnification to high magnification.

As a further restriction, the length reflected by one pixel in the lowest magnification (k_0 / A_{pixel}), has to be at least the same as the structural size s . Assuming that the ε -factor is 10%, the positioning accuracy should be half the size s .

Furthermore, if the object recognition accuracy is about 1% of the number of pixels ($A_{\text{Pixel}} = 500$), then the number of ZAC steps is the ceiling of the value calculated with Equation 2.3, thus $n = 2$. The first magnification step ($n = 1$) is then used for magnifying approx. 50 times, the second step ($n = 2$) for magnifying again approx. two times. From this typical example, it can be concluded that for applications where in the first magnification the object is just recognized, two ZAC steps are generally necessary to reach the desired magnification. With very good parameter sets, zooming and centering can be achieved in one step. For poor object recognition accuracies and number of pixels, the number of zoom steps increases to approximately three. Hence, in typical nanohandling applications, the **number of ZAC steps** is smaller than or equal to three.

Consequently, it should be considered that nanoscale handling processes contain **more tasks** compared to macroscale processes, as zoom-and-center steps occur more frequently.

2.2.3 SEM-related Issues

In the last section, the necessary number of ZAC steps was discussed. In the work space of SEMs, an increase in magnification implies a higher resolution, thus opening the possibility of substituting on-board position sensors by higher resolution SEM image acquisition and object recognition. This method has been used widely for the automation of nanohandling tasks [8, 9]. However, image acquisition takes longer than reading a sensor value; shorter image acquisition and processing times result in noisier images. Thus, the magnification where the on-board position sensor is replaced by object recognition has to be chosen taking the resolution enhancement as well as the delays into account.

2.2.3.1 Sensor Resolution and Object Recognition

The SEM is a high-resolution image acquisition unit and thus, as mentioned above, can be used as a sensor for closed-loop position control, substituting or supplementing an on-board position sensor (Figure 2.2). SEM object recognition challenges are discussed in Chapter 4. Issues regarding the position controller are considered in Chapter 3.

In Figure 2.3 a comparison between the resolution of a common on-board sensor for a linear axis and the achievable resolution using image processing and object recognition are plotted against the magnification of the SEM. It is clearly visible that already at magnification higher than 300 times in this case, the resolution achieved through object recognition is better than the on-board sensor resolution. Hence, with respect to image resolution, switching between the on-board position sensor and object recognition can occur when

$$\frac{k}{A_{\text{Pixel}}} \cdot u_{\text{Pixel}} < u_{\text{Sensor}} , \quad (2.4)$$

where A_{Pixel} is the number of pixels for the imaged square with edge length k , u_{Pixel} is the accuracy of object recognition in pixels, and u_{Sensor} is the sensor accuracy.

Thus object recognition is preferably used compared to the on-board sensors, if the resolution of the object recognition system is significantly better. Modern piezoactuators, stick-slip, or continuous actuators accomplish step widths of 10 to 20 nm. In most cases, therefore, the **sensor resolution is the bottleneck** rather than the actuator resolution.

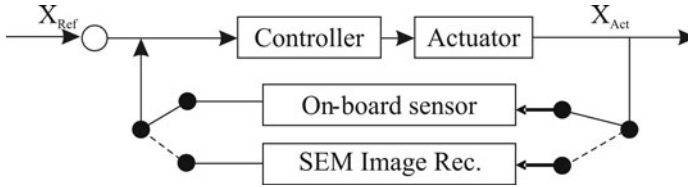


Figure 2.2. Typical control schematic for an actuator used for nanohandling automation. The on-board position sensor is substituted by SEM object recognition where the resolution is significantly better.

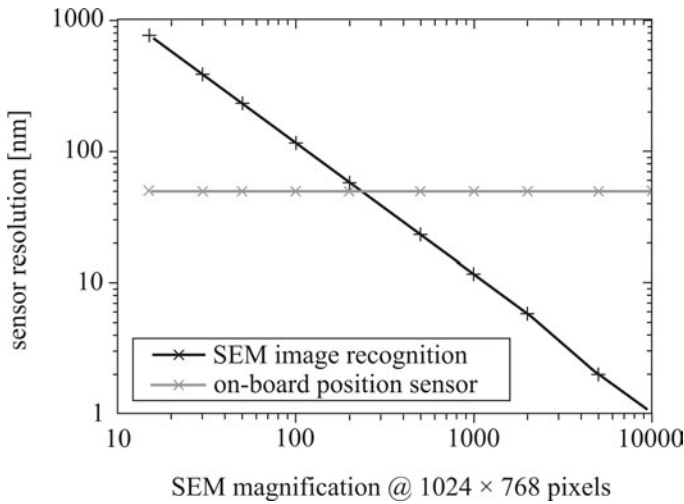


Figure 2.3. Comparison between the achievable sensor resolution using the on-board sensor of linear stick-slip axes and SEM object recognition. The on-board sensor is of type Numerik Jena L4 [10] and has an interpolated resolution of 50 nm, independent of the magnification. The resolution of SEM object recognition was measured according to the left side of Equation 2.4, using a recognition accuracy of 1 pixel.

2.2.3.2 Noise

The SEM as a scanning image sensor has a resolution of approx. 0.1 nm for field emission guns. These high resolutions are only achievable with comparatively long image acquisition times, when the signal-to-noise ratio is maximized. In general, the image quality is improved when scanning speed is reduced. However, for most automation processes, **high scanning speeds** combined with **fast object recognition** are desirable. Therefore, a compromise between these two aspects has to be chosen. The typical noise of an SEM image plotted against the scanning time is shown in Figure 2.4.

Obviously, it is necessary to increase the scan time if object recognition fails due to noisy images. For automation purposes, an update rate for sensor poses of 2 per second is tolerable, but a lower rate significantly slows down the process. A reduction of noise by the factor 0.5 leads to approx. 10 times longer scan times, whereas a reduction of the scan time to one third leads to three times more noise in the image. Thus, specialized methods for high update rates at high recognition reliability are necessary, which will be described in Chapter 4.

2.2.3.3 Velocity and Image Acquisition Time

The scanning speed also limits the maximum travel speed of an actuator, when object recognition is used as sensor feedback. Consider a point-like object under observation of a vision sensor with a frame refresh rate f_s , respectively a frame acquisition time T_s and a resolution A_{pixel} , given in pixels. The area under observation is assumed to have an edge length of k . Then the object recognition accuracy $u_{\text{recognition}}$ is determined by the following equation:

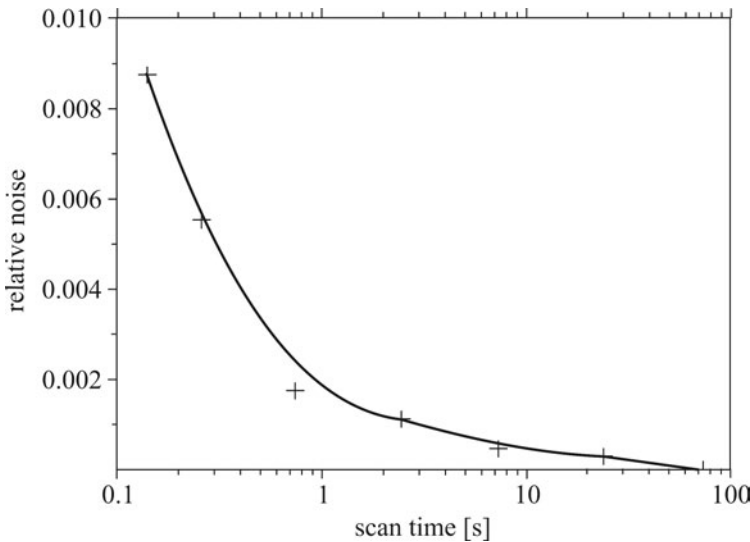


Figure 2.4. Relative noise of an SEM image for different scanning times at an image size of 512×442 pixels. The relative noise was calculated as mean-square error relative to the error at a maximum scan time of 73 s.

$$u_{\text{recognition}} = \frac{k}{A_{\text{Pixel}}} \cdot u_{\text{Pixel}}, \quad (2.5)$$

where u_{Pixel} is a constant depending on the system and taking into account how precisely the position should be recognized. Typical values range from 1 to 10, e.g., a value of 2, using the sampling theorem. The scan process is simplified here to be a process where the image is scanned line by line and the column-wise scanning within a line is neglected. Then, two cases have to be considered for estimating the maximum allowed velocity v_{max} of an object, if it has to be recognized at least in two subsequent images until the scanned area is left:

- The object is **moving orthogonal** to the scanning direction, *i.e.*, the time Δt between two occurrences of the object can be considered approx. T_s .
- The object is moving in the same direction as the scan is running. Then again two cases have to be considered: In the first, object movement and scan direction are **anti-parallel**. Then the time Δt until an object occurs in the following frame is shorter than the frame time T_s . For the second, the object's movement is **parallel** to the scan direction, resulting in longer time Δt between the occurrences in two successive frames. Then the maximum allowed velocity v_{max} can be calculated from the intersection of two lines, resulting in

$$v_{\text{max}} = \frac{1 - \frac{u_{\text{Pixel}}}{A_{\text{Pixel}}}}{2 \cdot T_s} \cdot k, \quad (2.6)$$

where T_s is the image acquisition and object recognition time. Taking for example a scan time of 0.5 s (*i.e.*, a sensor refresh rate of 2 Hz) at an edge length of the scan field of 50 μm and a recognition accuracy of 10%, then the speed limit according to the above equation would be $v_{\text{max}} = 45 \mu\text{m/s}$.

2.3 Automated Nanohandling: Problems and Challenges

2.3.1 Parasitic Forces

The expression “parasitic forces” is commonly used as the collective term for surface forces that have major relevance in the micro- and nanoscale, *i.e.*, van der Waals, electrostatic, and capillary forces.

Electrostatic forces refer to forces due to electric charging of objects. Two objects that are charged with the same polarity repel each other, whereas oppositional polarity leads to attraction. Typical causes for electrostatic forces in handling processes are contact electrification, triboelectrification, and direct charging through the electron beam in the SEM. Charging through the electron beam of an

SEM can lead to repelling forces, resulting in objects floating around on the substrate surface. Other observed effects are electrostatic actuators in the SEM driven by the electron beam or image artifacts occurring due to the electrostatic deflection of the primary beam. In [11], the equation for estimating the electrostatic force between a sphere of radius r with a charge q and a conductive plane in distance is given by

$$F_{el} = \frac{q^2}{4\pi\epsilon(2r)^2}, \quad (2.7)$$

where ϵ is the dielectric permittivity. In practice, the force is hard to estimate because in general neither the charge nor the dielectric permittivity are known. In the SEM, special measures preventing or minimizing charging through the electron beam can be taken, *e.g.*, observation in low-vacuum modus or optimization of the beam parameters.

Van der Waals forces denote the (attractive) forces between atoms and molecules due to interatomic forces and can be calculated for a sphere on a plane by the following equation [11, 12]:

$$F_{vdW} = \frac{h \cdot r}{8\pi z^2}, \quad (2.8)$$

where h is the Lifshitz-van der Waals constant and z is the atomic distance between the sphere and the plane. In [12], values for the Lifshitz-van der Waals constant are given for several material combinations, although this term is in general hard to estimate for handling processes.

Capillary forces are due to liquid films between two objects. Even in high-vacuum chambers, *e.g.*, when an SEM is used as vision sensor, liquid films on the surface of objects cannot be avoided. Due to water films (condensation), oil films (pump oil), *etc.*, the surfaces of objects, tools, and substrate can never be considered dry. Estimations for the capillary force between a sphere and a plane are given in [11, 13], resulting in the following equation:

$$F_{cap} = 4\pi r \gamma, \quad (2.9)$$

where γ is the surface tension. However, the capillary force between object and gripper has also been used successfully for gripping, thus using the parasitic effect for handling objectives [14-16].

Fearing surveyed the parasitic forces and their influence on parts below 1 mm size. In [11], he suggested the following actions, among others, for reducing the influence of adhesion forces:

1. Usage of conductive materials for reducing charging effects. In micro- and nanotechnology, silicon is, however, a very common material for handling

tools, which forms an insulating oxide. A work-around for this problem is covering the tools with a **conductive layer**, *e.g.*, gold, where possible.

2. **Rough gripper jaw surfaces** in order to minimize the contact area. This measure should even be adopted for the design of gripper jaws, which allow a minimum of point-point contacts between object and gripper. Furthermore, the gripper geometry should always be adapted to the object to be handled.

It can be concluded from the survey of parasitic forces that most of them are very hard to estimate. Many factors in a handling system are either unknown or hardly measurable, *e.g.*, the capillary forces due to condensed water in an SEM's vacuum chamber. The complexity regarding geometry and interactions between multiple objects in a handling system additionally complicate the calculation of parasitic forces. Furthermore, these forces are time-variant, *i.e.*, they can change dramatically during a handling process. For example, a silicon gripper charged through the SEM's electron beam can be discharged through contact with the substrate surface.

Thus the parasitic forces are the major problem for the automation of handling tasks on the micro- and nanoscale due to their uncertainty and time-variance [16]. Experimental observations [17, 18] proved this conclusion.

2.3.2 Contact Detection

One of the major issues in the handling and assembly of nanoscale parts is the detection of contact between two objects. The issue arises when 2D images, *e.g.*, from a light microscope or SEM, are used as global vision sensors determining the out-of-plane positions of objects relative to each other. Object recognition can be used for contact detection within the observed plane, but out-of-plane contact detection is not possible. A typical example is the detection of whether a gripper touches a probe surface. If this scene is observed from above, *e.g.*, with an SEM providing high depth of focus, it is hardly possible to distinguish with common image recognition tools if the gripper touches the surface or not. Possible approaches for solving this problem are presented briefly in the following paragraphs.

Depth from focus: The depth-from-focus method is described in [19, 20] for measuring the height difference between two objects by means of a focus sweep. For the series of images, two regions of interest containing both objects are defined. For every region and image, the variance is determined. The variance shows a local minimum in the variance function over the changing focus, where the object's sharpness is at its maximum. Based on this method, the difference in height between two (object) surfaces can be determined.

Touchdown sensor: This sensor [21-23] provides a method for measuring contact between two objects by means of a resonance method. The resonator consists of a piezoelectric actuator and a piezoelectric sensor, on which the tool, *e.g.*, a gripper, is mounted. The piezoelectric actuator oscillates very close to the resonance frequency of the system. The system's mechanical oscillation induces an

electrical current in the piezosensor. This current oscillates at the same frequency and with a certain amplitude. When the tool touches another object or a surface, the resonance frequency of the system changes, leading to a drop in the measured amplitude.

3D vision: The idea of creating a 3D image out of two SEM images recorded from different angles has been the subject of research for several years. Especially with regard to automation processes, it is obligatory to deflect the electron beam instead of the probe. A promising approach will be presented in Chapter 5.

Vision-based force measurement: Vision-based force measurement quantifies the deformation of a stressed object by means of object recognition [24, 25]. The algorithm can be applied for measuring forces – and thus contact – between two objects. For calculating the forces applied on an object, *a priori* knowledge is necessary, whereas for simple contact detection the deformation is evidence enough. However, this method is best applied where the object's stiffness is low, *e.g.*, measuring of contact or force between a gripper and a nanotube [26].

2.4 General Description of Assembly Processes

In this section, the process design and considerations with regard to serial assembly tasks on the nanometer scale will be given. Figure 2.5 provides an overview of the typical tasks that are necessary to accomplish an assembly process.

A description of the single tasks will be given in the next section. Based on this, further consideration regarding the reliability of assembly processes is given in the section after. Basically, simple handling tasks are the separation of an object, its transportation to another position and its release. Assembly processes comprehend (multiple) handling tasks, but are extended by joining processes and eventual inspection processes for quality assurance.

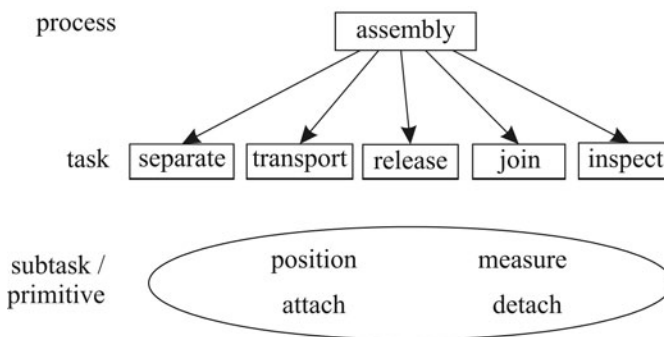


Figure 2.5. Overview of the tasks required in an assembly process. A typical process consists of the tasks “Separate”, “Transport”, and “Release”. Every task can again be separated into subtasks, which can be seen as primitives.

2.4.1 Description of the Single Tasks

The tasks and subtasks forming a process can be best described as a change between two quantifiable states A and B. Especially for nanohandling tasks, it is very important that these states are quantifiable by means of measurement values, *e.g.*, giving a position in coordinates or describing the contact between two objects. Hence, ideally, the process is always in a definite state. In the following subsections, elementary tasks will be described with respect to the special requirements of the nano- and the macroworld.

Separation: The separation task can be considered as the occasion when the object's attachment status is changed, *i.e.*, in the beginning its condition is "connected to substrate" and at the end of the process it is connected to a tool or an intermediate product. The task itself can be achieved by several methods, *e.g.*, gripping and lifting, gluing and etching. Already from these examples it is obvious that the separation task includes at least two subtasks, *i.e.*, connecting the object to the tool and releasing the object from the substrate.

The separation of objects is one of the most difficult tasks in the field of nanohandling (Figure 2.6). The main reasons are the influences of parasitic forces and the comparatively weak forces which can be exerted by grippers or similar tools. An overview of strategies for lifting off small objects on the nanoscale, *e.g.*, nanowires, is given in [6, 17].

Transport: The transport task differs from macroscale transport tasks simply by the possible number of orders of magnitude in geometric scale, but is conceptually the same: the gripped or previously fixed object is transported from position A to a position B. Care has to be taken that the object is not released by accident during transport, *e.g.*, caused through vibrations of the actuators. A further description of positioning issues and position control will be given in Chapter 3 and Section 2.6.

Release: The "release" task is the reverse of "separation", *i.e.*, at first the object is attached to the substrate and then the object is detached from the tool. The parasitic forces cause an object on the nanoscale to stick to handling tools until the forces between the surface, where the object should be placed, are higher than the forces between the tool and the object. A reduction in sticking forces can be achieved using two principal ways:

1. The sticking force is reduced by **reducing the contact size**, *e.g.*, through specially formed gripper jaws or by reducing the influence of the parasitic forces, *e.g.*, through special coatings on the jaws. These measures usually require a considerable technical effort.
2. Instead of adapting the gripper to the gripping task, a **special technique** for releasing the object can be applied, *e.g.*, wiping off [17] or shaking off. Both techniques aim at shifting the balance between gripper-object forces and object-substrate forces to the substrate side.

Joining: The joining of objects is the central task for assembly processes. In principle, three different methods can be used for joining objects:

1. **Material closure:** two objects are connected using a material connection between both, *e.g.*, welding, gluing, or soldering. In Chapter 10, electron beam induced deposition (EBiD) will be explained in more detail, as it is a very promising method for joining parts through material closure inside the SEM.
2. **Force closure:** two objects are connected by a force, which can also be a parasitic force [27].
3. **Form closure:** two objects are joined by their geometry. This approach is not very common in nanoassembly tasks.

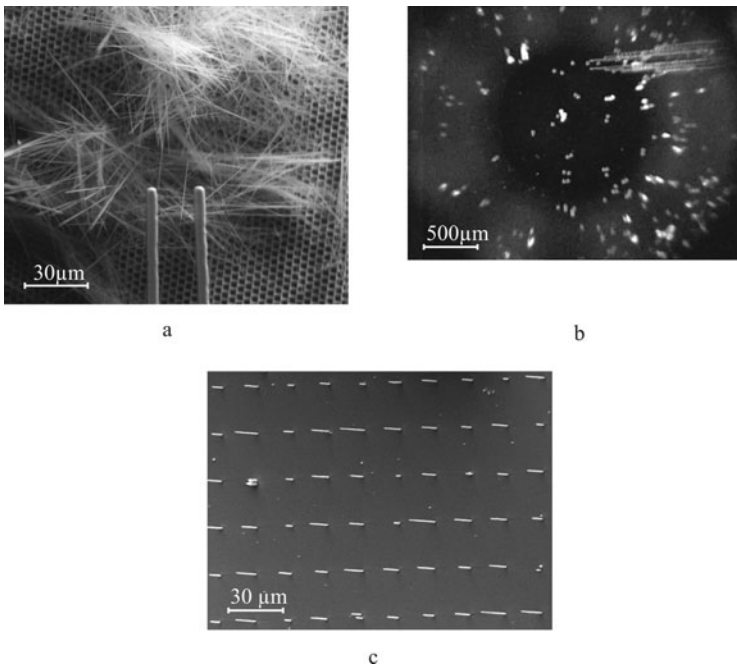


Figure 2.6. Typical objects to be manipulated in micro- and nanohandling tasks. a. A gripper trying to grab one out of a bunch of silicon nanowires in the SEM. The nanowires with a diameter between 200 and 500 nm and a length of several micrometers have been put on the substrate simply by peeling off. This separation task is very hard to automate, due to the parasitic forces holding the nanowires together. b. A glass ball (diameter approx. 30 μm) has to be gripped by a silicon gripper in the light microscope. This task can be automated, because the balls are split up and do not adhere to the surface due to the reduced contact area. c. CNTs grown in a matrix on a silicon wafer. This is a good starting point for automation processes, as the nanowires are separated and orientated on the wafer. However, they have to be detached from the substrate by breaking or etching.

Inspection: The inspection task serves for quality assurance. Many parameters can be tested to prove that the assembly process has been successful: stressing the connection up to a threshold force, chemical analysis of deposited material, electrical characterization of the bonding through resistance measurements.

2.4.2 General Flowchart of Handling Processes

Based on the simple tasks described above, it is possible to set up more complex processes, *e.g.*, handling and assembly by combining these to a **linked task chain**. Generally, every process, task, and subtask can be described in the process flow chart as a change from condition A to condition B. The conditions can be described as a vector containing the position data of single components, *i.e.*, objects and tools, and their relation to each other, *e.g.*, “part 1 connected to part 2”. Based on these measurable values, it is possible to **trace failures** that would result in a process failure. Figure 2.7 shows the main tasks needed for bonding a CNT to an AFM tip. Additionally, the number of subtasks needed for successfully fulfilling a task is given.

2.5 Approaches for Improving Reliability and Throughput

2.5.1 Improving Reliability

The reliability of the overall process $R_{process}$ for a series of subtasks can be calculated by multiplying the single subtask reliabilities, *i.e.*,

$$R_{process} = \prod_{i=1}^n r_{subtask_i} = \overline{r_{subtask}}^n, \quad (2.10)$$

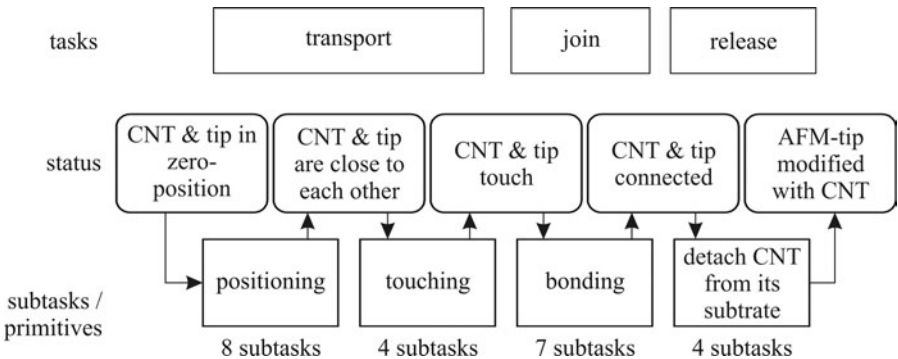


Figure 2.7. Typical process layout for bonding a single CNT to an AFM tip, showing the conditions between the tasks, the tasks and the number of subtasks for every task

where $r_{subtask_i}$ is the reliability of the i -th subtask and n is the amount of subtasks. For example, a mean reliability $r_{subtask}$ of 98% for the 23 subtasks shown in Figure 2.7, leads to an over-all reliability for the process of 63%. A further decrease of the mean reliability for the subtasks down to 95% reduces the over-all reliability to 31%. This example shows the importance of maximizing the subtask reliability on the one hand and minimizing the number of subtasks on the other.

Another means, which is of special interest for serial assembly processes, is the definition of fallback markers in the process chain. If a task or a subtask fails, the system should be brought into a defined state, from where the chain can be continued. This method is referred to as **failure analysis with non-ambiguous retrace**.

Minimizing the number of subtasks: For minimizing the number of subtasks, several measures can be adopted:

1. Skillfully planning the handling tasks. This can be achieved through reducing the number of tools needed. One very important consideration, which should be taken into account for assembly tasks, is, *e.g.*, the omission of a gripper. This reduces the number of tasks substantially, because intermediate tasks, which are not directly concerned with connecting two objects to each other, can be left out. For example, connecting CNTs to AFM tips is a process where the gripper can be left out, if the CNTs come in a suitable pre-packaged orientation (Figure 2.6c).
2. Optimizing the number of subtasks needed for fulfilling a task. A typical example is minimizing the number of necessary ZAC steps (Section 2.2.2). Further improvements can be achieved if, *e.g.*, position sensors providing very high resolution over a wide scale are used. This prevents the switching of sensors and thus leads to a reduction of subtasks for the same positioning task.

Maximizing subtask reliability: subtask reliability can be increased using the following measures:

1. Continuous application of sensors, ideally setting up of closed-loop control systems, in order to trap exceptions. *In situ* measurement methods are of special interest for controlling subtasks.
2. Attaching and detaching subtasks are of special interest in terms of reliability. Based on the indetermination of parasitic forces, form and force closure should be substituted through material closure where possible, *e.g.*, bonding TEM lamellae to tips instead of gripping them with mechanical grippers.

2.5.2 Improving Throughput

The throughput D of the process can be defined as the inverse of the mean time needed for one process $T_{process}$, *i.e.*,

$$D = \frac{1}{\overline{T}_{process}}. \quad (2.11)$$

For estimating the influence of single parameters, the following assumptions are made: a process consists of n subtasks, with a mean duration $\overline{T}_{subtask}$ and a mean reliability $\overline{r}_{subtask}$ each. Every subtask is repeated until it has succeeded and thus the whole process is successful. For a large number of equal processes, the mean process duration can then be calculated from

$$\overline{T}_{process} = \frac{n \cdot \overline{T}_{subtask}}{\overline{r}_{subtask}}. \quad (2.12)$$

From this equation, the influence of the single parameters on the throughput can be qualified. For maximizing the throughput of a process, it is thus necessary to minimize the number of subtasks and to maximize the subtask reliability. Both measures have already been discussed in the section above. However, for minimizing the mean duration $\overline{T}_{subtask}$ of a subtask, the following measures can be taken:

1. **Optimizing the travel speed** of actuated parts through fast sensors. Additionally, as scanning vision sensors are widely used for nanohandling, the optimization of image acquisition and recognition has to be taken into account.
2. Especially for handling tasks, where the separation task is often very critical, the duration can be minimized by **optimizing the layout of the stored objects**.
3. Contact detection can be one of the very time-consuming tasks, because the travel speed of the actuators has to be reduced, in order to prevent hard crashes. Therefore, **vision-based methods** for the determination of the distance between object and tool, respectively substrate, are preferred. One approach, 3D vision sensors, is discussed in Chapter 5.
4. **Optimizing controllers for speed**, as discussed in Chapter 3.

2.6 Automated Microrobot-based Nanohandling Station

The **automated microrobot-based nanohandling station** for TEM lamellae handling was one of the first implementations of the generic AMNS concept presented in Chapter 1. The station was developed by the Division Microrobotics and Control Engineering (AMiR), University of Oldenburg, in the framework of the EU project ROBOSEM (grant number GRD1-2001-41861). The main purpose of the project was the integration of microrobots as well as position and force sensors into the vacuum chamber of an SEM. The client-server-based control system supports the user during nanohandling processes, where the objects' sizes range from some

hundred μm to some hundred nm. A good example that has evoked interest from industrial partners is the handling of silicon lamellae that are to be evaluated in a TEM.

2.6.1 AMNS Components

2.6.1.1 Setup

The setup of the nanohandling station (schematic in Figure 2.8 and picture in Figure 2.9) consists of one microrobot that positions the sample to be handled (“sample robot”), and one microrobot that positions the end-effector, performing the actual handling task (“handling robot”) [9, 28, 29]. Besides the main sensor, the SEM with image processing, CCD cameras with image processing, a position sensor, and a sensor for contact detection (“touchDown sensor”) are employed to support the user and to allow for automatic positioning. The setup is attached to an exchangeable door of the SEM, so that it can be assembled, maintained and tested outside the vacuum chamber with a light microscope as SEM replacement. This reduces valuable SEM time, avoids pump time for the vacuum and generally allows for easy access to all components.

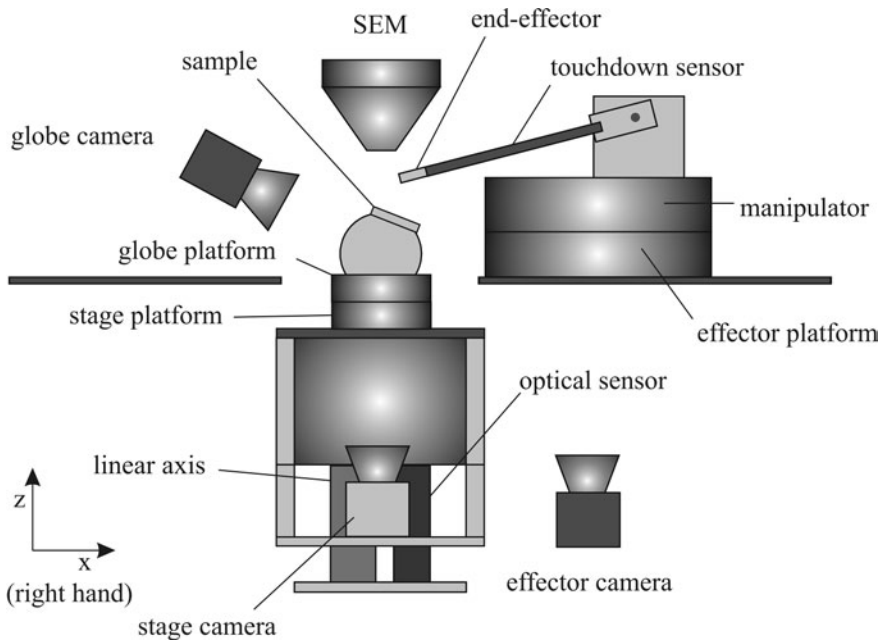


Figure 2.8. Schematic of the nanohandling station. The sample robot consists of the stage platform with a sphere carrying the specimen. It can position the sample in all six DoF. The handling robot consists of the effector platform with the manipulator carrying the touchdown sensor and a gripper. It can position the end-effector in the three DoF of a horizontal plane. The two translational DoF have a high actuation resolution.

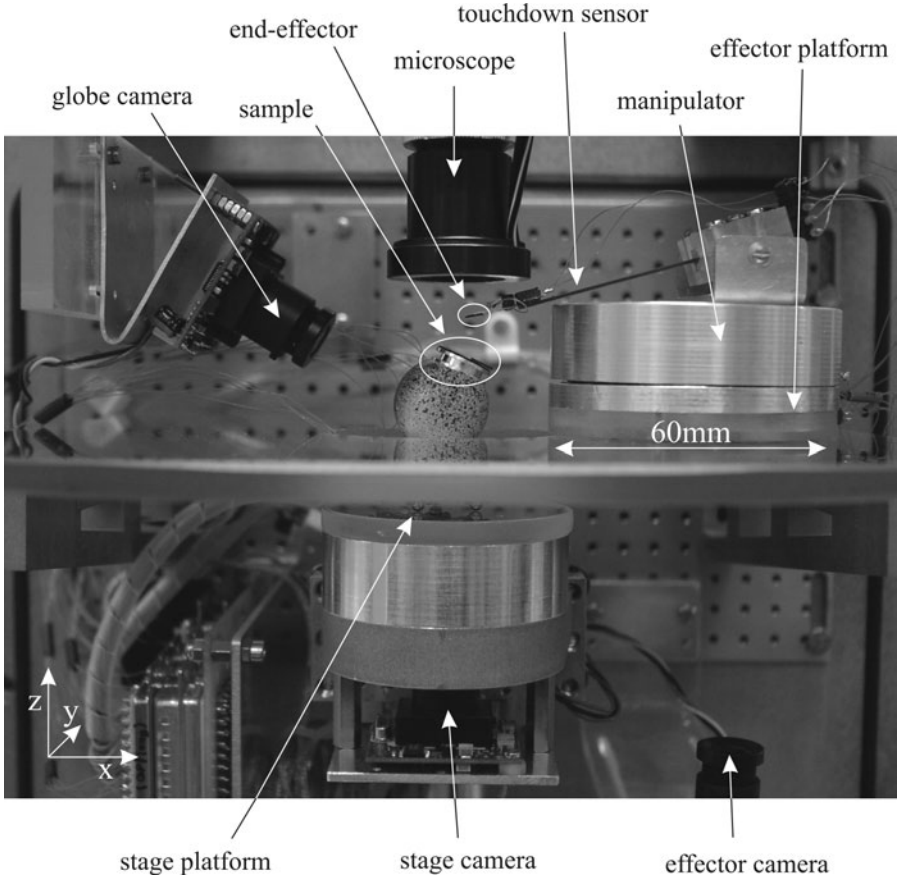


Figure 2.9. Setup of the nanohandling station. For development purposes, a light microscope is used and removed when the station is used in the SEM.

2.6.1.2 Actuators

The **sample robot** consists of two single-disk mobile platforms (diameter: 30 mm) and a linear axis. One mobile platform (**stage platform** in Figure 2.8) moves on a horizontal glass plate and carries another platform (**globe platform**), which is mounted upside down to rotate the sphere-shaped sample holder in all three rotational degrees of freedom (DoF). The working principle of the mobile platforms is explained below. The mobile platforms holding the sample can be moved vertically with a piezo-based **linear axis** from [30], which is fixed to the SEM door. Using all components of the sample robot, the sample can be positioned in all six DoF.

The **handling robot** consists of a triple-disk mobile platform (diameter: 60 mm), which carries a manipulator with an end-effector, *e.g.*, a gripper. The mobile platform (**effector platform** in Figure 2.8) moves on a separate horizontal glass plate around the sample robot to coarse-position the end-effector, and the **manipulator** then positions the end-effector with higher resolution to its desired (x, y) -position. The manipulator consists of two piezo stack actuators, which drive

leverage arms fixed by flexible hinges. The maximum stroke of the table is about $40\text{ }\mu\text{m}$. The **end-effector** can thus be positioned in x and y with high resolution, and rotated around the z -axis. The end-effector itself can be passive, like an STM (scanning tunneling microscope) tip, or an AFM cantilever, or active like a microgripper from [31], or from the Technical University of Denmark, Lyngby, Denmark (Chapter 7).

2.6.1.3 Mobile Microrobots

Two different implementations of a mobile microrobot platform are integrated into the AMNS [32-34]. The **triple-disk platform** is actuated by three piezodisks, which are each segmented into three parts (Figure 2.10a and c). A small ruby bead is glued to each segment, and each three-tuple of ruby beads drives one of three metal or sapphire spheres, which support the mobile platform. Instead of three piezodisks with three segments each, the **single-disk platform** consists of one piezodisk with nine segments (Figure 2.10b and d). In the setup, the triple-disk platform implements the effector platform while the single-disk platform implements the stage platform and the globe platform.

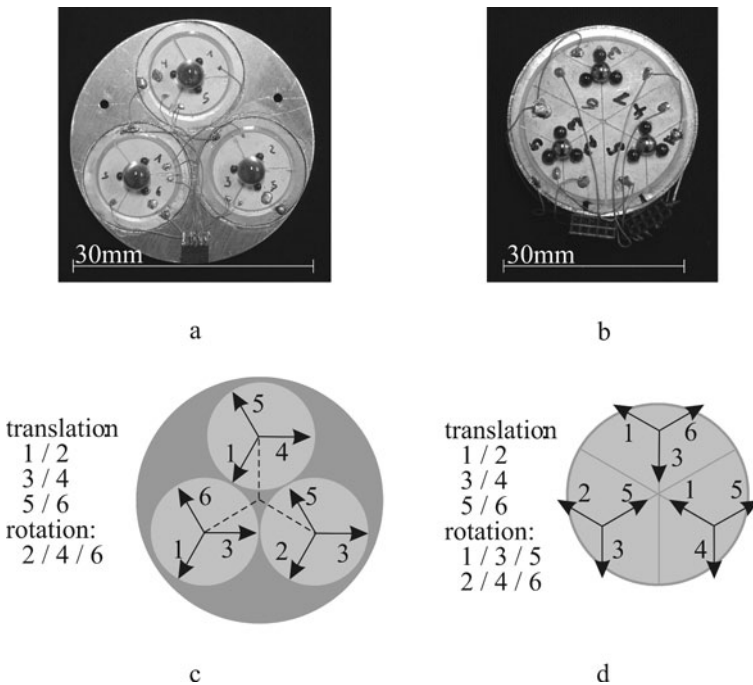


Figure 2.10. The triple-disk platform with three piezodisks: a. bottom view and c. channel configuration. The single-disk platform with one piezodisk: b. bottom view and d. channel configuration.

The developed platforms make use of the **stick-slip principle** by applying a voltage signal, which consists of a part with a gentle slope and a part with a steep slope, such that the segments are bent correspondingly slowly and fast (Figure 2.11). During the slow bending, the small ruby bead moves the large sapphire sphere, leading to a small rotation. This is called the stick phase. During the fast bending, the small ruby bead slides over the sapphire sphere, which therefore keeps its orientation. This is called the slip phase.

The number of control channels is reduced from nine to six by electrically connecting each of three piezo segment pairs. The configurations given in Figure 2.10c and Figure 2.10d yield three principal translation directions and one principle rotation direction, such that the microrobot platforms can move in all three degrees of freedom.

2.6.1.4 Sensors

The main high-resolution sensor of the nanohandling station is a LEO 1450 SEM [35], in combination with image processing, which provides “poses” of micro- and nanoobjects and end-effectors with resolutions down to 2 nm (magnification

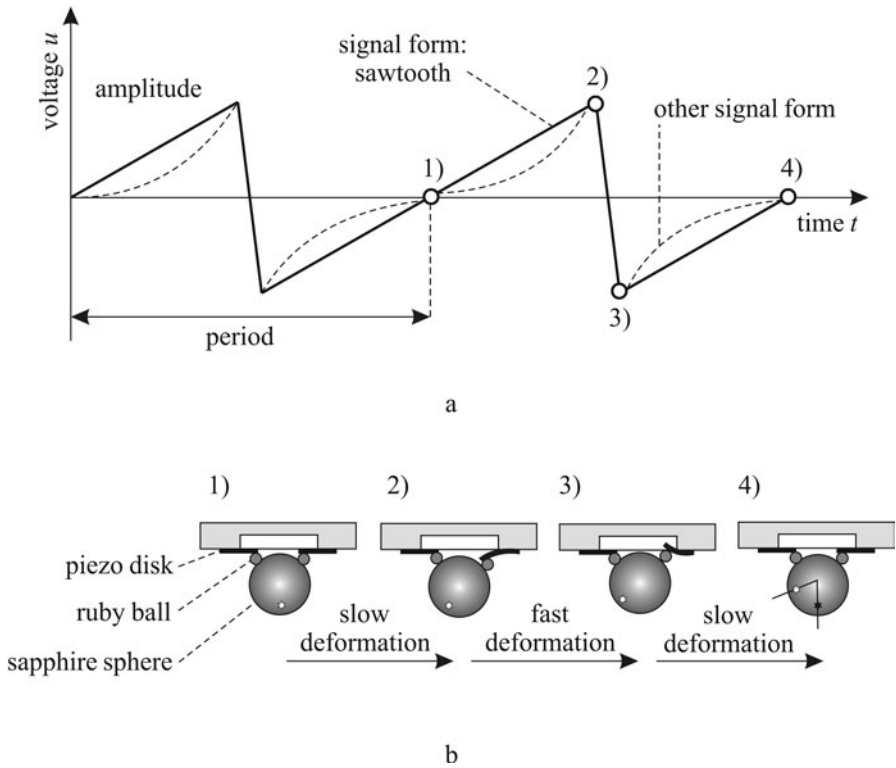


Figure 2.11. a. Typical voltage signal that is applied to a piezo segment. b. Stick phase by slow deformation and slip phase by fast deformation of the piezo segment.

50,000 \times , fast scanning). The generated pictures are acquired using the digital image acquisition unit offered by [36] and are processed using algorithms that have been developed at the AMiR [37-39]. For the coarse positioning of the mobile platforms, three corresponding **CCD cameras** are mounted on the SEM door. Together with the image processing software developed at the AMiR, they measure the mobile platform's poses with resolutions of about 60 μm (stage camera) and 170 μm (effector camera).

Measurements in the vertical direction are performed with two sensors. An optical **position sensor** from [40] measures the z -position of the linear axis with respect to a fixed reference (resolution below 1 μm). In addition, a **touchdown sensor** detects when the end-effector touches another object, *e.g.*, a microobject to be handled [9]. The touchdown sensor is a bimorph piezo-bending actuator, which is attached to the manipulator, and acts as a cantilever holding the end-effector. One ceramic layer is driven by an AC voltage with small amplitude (5 mV), and the other layer measures the amplitude of the resulting mechanical oscillation (approx. 50 nm). A contact between end-effector and microobject then results in a considerable and distinct drop in the measured amplitude.

2.6.1.5 Control Architecture

The control system is set up as client-server architecture with communication over TCP/IP to allow for flexible use of the control and sensor modules in different applications (Figure 2.12).

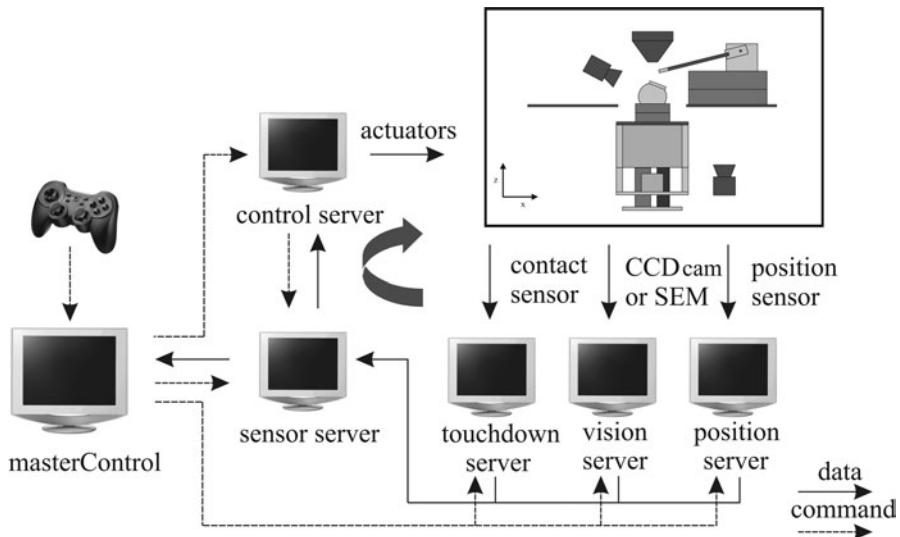


Figure 2.12. Control system architecture of the nanohandling station (a detailed view of the inlay figure in given in Figure 2.8). The touchdown server, the vision server, and the position server send their measurement data to the sensor server. The control server requests the measurement data when needed to control the actuators. The super-client master control controls all servers remotely and provides an interface to the user.

On the sensor side, there is a **vision server** that is responsible for the acquisition and processing of images from the SEM and from the CCD cameras. Its task is to detect features of microobjects, end-effectors, or microrobots and to determine their pose in a global frame (Chapter 4). Also, the optical position sensor and the touchdown sensor have their own server applications (**touchdown server** and **position server**). All servers continuously send their data to a **sensor server**, which stores the most recent data of each sensor and which provides that data to any client requesting it. On the actuation side, a low-level **control server** is responsible for the access of the actuation hardware and for the execution of control primitives with sensor feedback via the sensor server. The most common process primitive is positioning an object like an end-effector with feedback from a microscope. The **master control** module serves as a super-client and controls all servers remotely. For the vision servers, it remotely chooses between different tracking models and input sources, and starts and stops the tracking and defines regions of interest. The touchdown server and the position server can be switched on and off remotely. For monitoring, the master control module continuously requests data from the sensor server about the microrobots' poses. On the control server, it remotely starts and stops the execution of low-level control primitives and forwards data from a teleoperation device. The user can control the microrobots via teleoperation or in a semi-automated way by triggering process primitives. The user receives status and position feedback from the graphical user interface of the high-level control module or visual feedback from the vision servers.

2.6.1.6 User Interface

The user can interact with the AMNS via a **graphical user interface** (GUI) and via a **teleoperation device**. In addition, an **emergency stop button** stops all actuators by disconnecting them from the power supply.

The **GUI** is the main part of the master control module and allows control of the connection to the servers and automation, supports teleoperation and gives information for monitoring (Figure 2.13). The **connection** part effects connection to, and disconnection from, the servers. The servers are identified by their IP addresses and their constant port numbers. The **automation** part effects the triggering of a predefined sequence of process primitives. Depending on the current automation state, it is possible to start this sequence at different intermediate states. An additional **calibration** provides a comfortable read-out and saving of different desired poses. For example, the pose of the effector platform, at which the connected gripper is in the SEM's field of view, can be reached by teleoperating the platform accordingly. The current pose can then be used by the automation module as the desired pose when coarse-positioning the gripper. The **pose** part can show the pose values of all sensors, which are connected to the sensor server. The **teleoperation and sensor control** part shows the current sensor and the current actuator and allows changing them. Controlled by a **cordless gamepad**, the current actuator can be moved in any desired direction and with any desired velocity. The maximum velocity can be adjusted in a wide range from constant movement to a

single step. Furthermore, the current sensor and actuator can be changed by the gamepad. Finally, in the **system messages** part, there is a textual output about the current and the last tasks.

2.6.2 Experimental Setup: Handling of TEM Lamellae

The control system can be seen as a tool to support user-performed nanohandling tasks in a teleoperated or in an automatic mode. Within the framework of the ROBOSEM project, the nanohandling station has been used to demonstrate the **semi-automated handling of lamellae**.

The handling sequence comprises the automated and teleoperated positioning of mobile microrobots. The names of actuators and sensors of the following sequence steps refer to the description above:

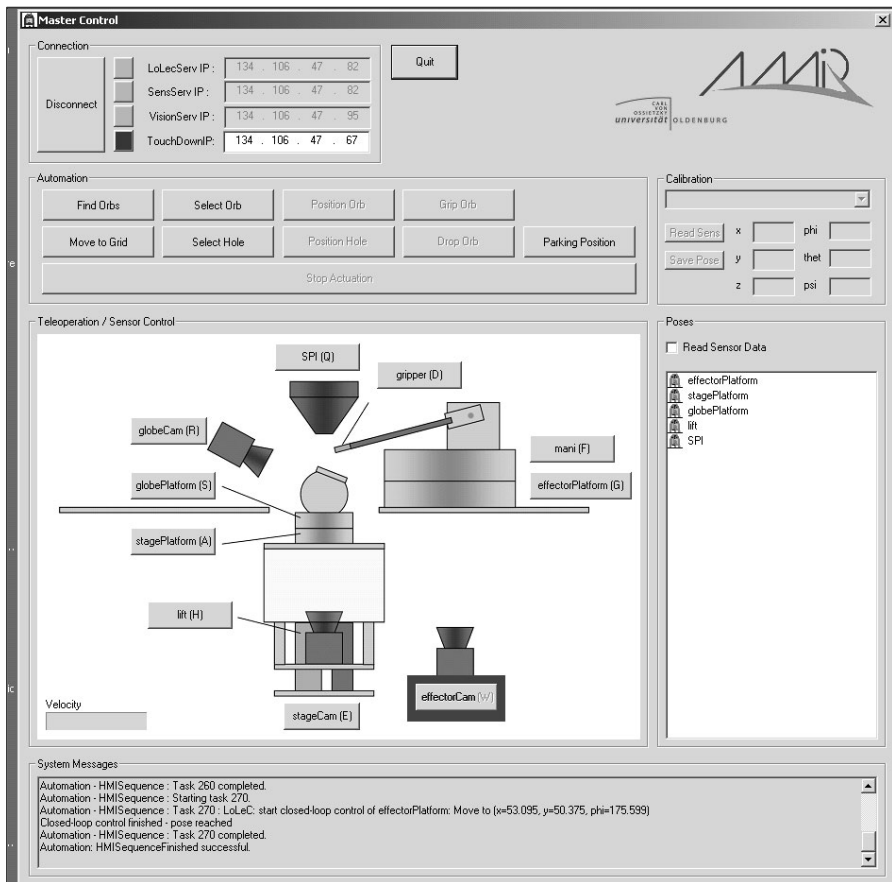


Figure 2.13. Graphical user interface of the AMNS

- **Lamella selection.** The sample, a silicon chip with four lamellae, is placed on the sphere, which can be rotated by the globe platform. First, the sample is coarse-positioned into the SEM's field of vision by moving the stage platform to a predefined pose with respect to the stage camera. The user then selects one of the lamellae, which is detected in the SEM image (Figure 2.14a).
- **Automatic lamella positioning.** The selected lamella is successively fine-positioned at a pose that allows good gripping with SEM feedback at magnifications of $50\times$, $300\times$, and $1000\times$ (Figure 2.14b, c, and d).
- **Automatic gripper positioning.** To avoid a collision during the gripper positioning, the lamella is lowered by some $100\text{ }\mu\text{m}$ using the linear axis with feedback from the optical sensor. The gripper is then coarse-positioned into the SEM's field of vision by moving the effector platform to a predefined pose with respect to the effector camera, followed by a successive fine-positioning with SEM feedback at magnifications of $50\times$ and $300\times$ (Figure 2.15a and b). The most accurate positioning of the gripper is then achieved by using the manipulator with feedback from the SEM. For gripping, the lamella is lifted up again, until the touchdown sensor detects a contact between gripper and specimen (Figure 2.15c).
- **Lamella gripping.** The lamella is gripped in teleoperation mode since the mismatch of the gripper's stiffness and the lamella's pull-off force leads to low gripping reliability (Figure 2.15d).

The lamella can then be transported to a TEM grid, which is placed on the same sample holder. The sequence is similar to the gripping sequence, *i.e.*, the positioning of TEM grid and gripper can be done automatically with feedback from

Table 2.2. Positioning accuracies during different tasks when handling lamellae

Task	Actuator	Meas. frame	Positioning accuracy			
			x [μm]	y [μm]	z [μm]	φ [$^\circ$]
lamella coarse positioning	stage platf.	Stage camera	20	20		0.5
lamella fine positioning	stage platf.	SEM (world)	2	2		
gripper coarse positioning	effector platf.	Effector camera	20	20		0.5
gripper fine positioning	effector platf.	SEM (world)	1	1		
gripper fine positioning	manipulator	SEM (world)	0.5	0.5		
lamella coarse positioning	linear axis	optical sensor			1	

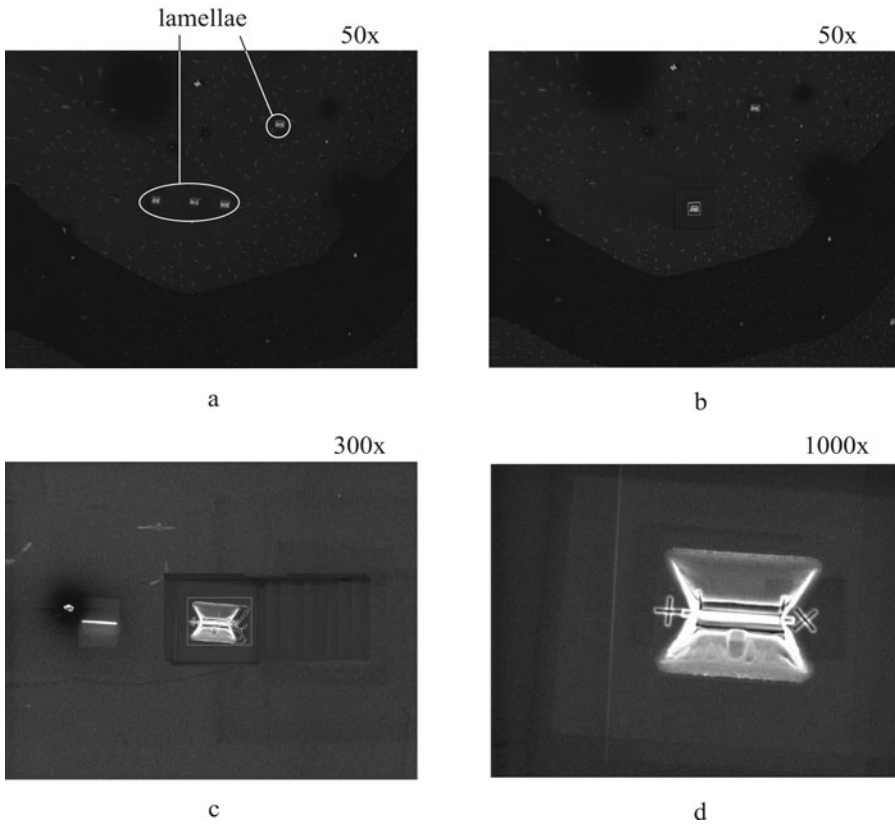


Figure 2.14. a. Selection of one of four lamellae. Successive positioning of the selected lamella with SEM feedback with magnifications of b. 50 \times , c. 300 \times and d. 1000 \times . Size of the lamella: 20 μm \times 10 μm \times 100 nm.

cameras, SEM, and touchdown sensor, while the actual release process must be carried out by teleoperation.

Table 2.2 lists the achieved positioning accuracies during different tasks when handling TEM lamellae. The accuracies are given with respect to the sensors which provide the feedback. For example, the gripper that is attached to the effector platform is positioned with an accuracy of 1 μm with respect to the SEM (gripper fine positioning in Table 2.2). The world frame is set to be the SEM image frame such that poses for the gripper and for the lamella can be used without any transformations. Moreover, the positioning accuracies that are given in Table 2.2 are the thresholds for the controller to stop the corresponding positioning process. They are chosen rather conservatively to increase the overall robustness and speed of the handling process.

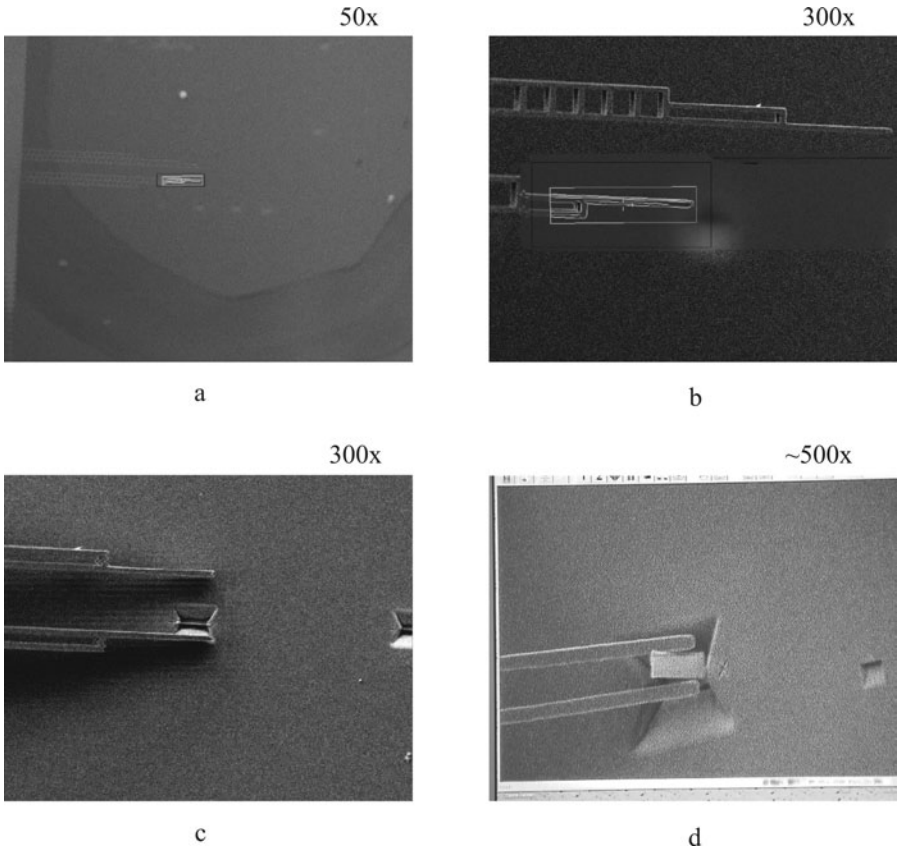


Figure 2.15. Positioning of the gripper with SEM feedback with magnifications of a. 50× and b. 300×. c. lift-up of the lamella with feedback from touchdown sensor. d. teleoperated gripping of the lamella. Gripper opening: 50 µm.

2.7 Conclusions

Vision sensors are essential for nanohandling tasks. A reasonable choice due to its good resolution, reasonable image acquisition times, and scalability is the **scanning electron microscope**. The SEM provides the possibility of substituting on-board position sensors and thus extending the closed-loop positioning resolution of a sensor-actuator system. The seamless zooming over several orders of magnitude is especially advantageous for automation, because typically more than one zoom-and-center step is necessary for accomplishing a handling or assembly task on the nanoscale. The number of necessary ZAC steps can be quantified to determine and optimize the overall number of process tasks. When applying SEM-based pose measurement in a closed-loop control structure, however, there is a trade-off between long image acquisition times and noisy

images. The image acquisition time determines the maximum allowable velocity of the actuators and the noise determines the reliability of the object tracking.

There are two major challenges regarding automated nanohandling. Firstly, inevitable and time-variant **parasitic forces** result in ambiguous behavior of objects. Possible approaches are the avoidance of grippers and the performance of handling tasks with material closure between object, tool, and substrate. Secondly, a reliable method for the **automatic detection of contact** between tools, objects, and substrate must be found. Possible approaches are depth-from-focus methods, the touchdown sensor concept, 3D SEM vision, and vision-based force measurement.

For the **optimization** of automated nanohandling and assembly **processes**, the **reliability** of each task can be **improved**. This can be accomplished by reducing the number of tasks and subtasks, by maximizing each subtask's reliability (closed-loop control, constant monitoring, *in situ* measurement), and by applying material closure for attaching and detaching subtasks. Furthermore, the throughput can be improved by prearranging parts for an optimized separation, by using a fast method for contact detection, and by maximizing the velocity of actuated parts.

Finally, the concept of an **automated microrobot-based nanohandling station** has been demonstrated for the handling of TEM lamellae, which integrates all essential components named above. An SEM and CCD cameras, together with dedicated image processing, are used as position sensors, which provide the feedback for the closed-loop control of different microrobots. Mobile platforms are applied for coarse positioning and piezostack actuators for fine positioning. A touchdown sensor detects contact between gripper and substrate. The communication framework for the sensors and actuators is a designed TCP/IP-based distributed control system. The separation, transportation, and release tasks are implemented, although separation proved to be difficult due to the parasitic forces, to the low gripping force, and to the low stiffness of the gripper.

The future activities aim at **improving reliability and throughput** for automated handling on the nanoscale. EBiD will be used as a reliable joining technique, avoiding grippers where possible. A very important step towards reliable processes on the nanoscale is the application of subtask **failure analysis and non-ambiguous retrace**, as well as a final inspection task for the quality assurance. Different contact detection methods will be evaluated with respect to reliability and speed. The communication framework is currently being redesigned and will use the common object request broker architecture (CORBA), which allows the integration of modules on different platforms and written in different programming languages. Finally, a script-language-based high-level controller allows flexible execution of different nanohandling processes with the same system (Chapter 7).

2.8 References

- [1] Clevy, C., Hubert, A. & Chaillet, N. 2006, 'Micromanipulation and micro-assembly systems', *International Advanced Robotics Programme (IARP) 2006*.
- [2] Böhringer, K. F., Fearing, R. S. & Goldberg, K. Y. 1999, 'Microassembly', *Handbook of Industrial Robotics*, 2nd edn, Shimon Y. Nof (ed.), pp. 1045–1066.
- [3] Dzenis, Y. 2004, 'Spinning continuous fibers for nanotechnology', *Science*, vol. 304, no. 5679, pp. 1917–1919.
- [4] Nelson, B. & Yu Zhou Vikramaditya, B. 1998, 'Sensor-based microassembly of hybrid MEMS devices', *Control Systems Magazine, IEEE*, vol. 18, no. 6, pp. 35–45.
- [5] Brufau-Penella, J., Puig-Vidal, M., López-Sánchez, J., Samitier, J., Driesen, W., Breguet, J.-M., Gao, J., Velten, T., Seyfried, J., Estaña, R. & Woern, H. 2005, 'MICRoN: small autonomous robot for cell manipulation applications', *Proceedings of IEEE International Conference on Robotics and Automation (ICRA)*.
- [6] Fukuda, T. & Arai, F. D. 2003, 'Assembly of nanodevices with carbon nanotubes through nanorobotic manipulations', *Proceedings of the IEEE*, vol. 91, no. 11, pp. 1803–1818.
- [7] Humphris, A. D. L., Miles, M. J. & Hobbs, J. K. 2005, 'A mechanical microscope: High-speed atomic force microscopy', *Applied Physics Letters*, vol. 86, no. 3, p. 034106.
- [8] Sievers, T. 2006, 'Global sensor feedback for automatic nanohandling inside a scanning electron microscope', *Proceedings of IPROMS NoE Virtual International Conference on Intelligent Production Machines and Systems*, pp. 289–294. Received the Best Presentation Award.
- [9] Fatikow, S., Wich, T., Hülsen, H., Sievers, T. & Jähnisch, M. 2007, 'Microrobot system for automatic nanohandling inside a scanning electron microscope', *IEEE-ASME Transactions on Mechatronics*, accepted.
- [10] Numerik Jena GmbH Germany, 2007, 'Datasheet for Encoder Kit L4', Online: http://numerik.itool4.net/frontend/files.php4?dl_mg_id=221&file=dl_mg_114422%6420.pdf.
- [11] Fearing, R. 1995, 'Survey of sticking effects for micro parts handling', *iros*, vol. 2, p. 2212.
- [12] Krupp, H. & Sperling, G. 1966, 'Theory of adhesion of small particles', *Journal of Applied Physics*, vol. 37, no. 11, pp. 4176–4180.
- [13] Hecht, L. 1990, 'An introductory review of particle adhesion to solid surfaces', *Journal of the IES*.
- [14] Lambert, P. D. 2005, 'A study of capillary forces as a gripping principle', *Assembly Automation*, vol. 25, no. 4, pp. 275–283.
- [15] Driesen, W., Varidel, T., Régnier, S. & Breguet, J.-M. 2005, 'Micro manipulation by adhesion with two collaborating mobile microrobots', *Journal of Micromechanics and Microengineering*, vol. 15, pp. 259–267.
- [16] Zhou, Q. 2006, 'More confident microhandling', *Proc. Int. Workshop on Microfactories (IWMF'06)*, Besancon, France.
- [17] Mølhave, K., Wich, T., Kortschack, A. & Boggild, P. 2006, 'Pick-and-place nanomanipulation using microfabricated grippers', *Nanotechnology*, vol. 17, no. 10, pp. 2434–2441.
- [18] Fatikow, S., Wich, T., Hülsen, H., Sievers, S. & Jähnisch, M. 2006, 'Microrobot system for automatic nanohandling inside a scanning electron microscope', *Proceedings of IEEE International Conference on Robotics and Automation (ICRA)*.

- [19] Estana, R., Seyfried, J., Schmoeckel, F., Thiel, M., Buerkle, A. & Woern, H. 2004, 'Exploring the micro- and nanoworld with cubic centimetre-sized autonomous microrobots', *Industrial Robot*, vol. 31, no. 2, pp. 159–178.
- [20] Watanabe, M., Nayar, S. K. & Noguchi, M. N. 1996, 'Real-time computation of depth from defocus', *Proc. of SPIE: Three-Dimensional and Unconventional Imaging for Industrial Inspection and Metrology*, vol. 2599, pp. 14–25.
- [21] Arai, F., Motoo, K., Kwon, P., Fukuda, T., Ichikawa, A. & Katsuragi, T. 2003, 'Novel touch sensor with piezoelectric thin film for microbial separation', *IEEE International Conference on Robotics and Automation, 2003. Proceedings. ICRA '03.*, Vol. 1, pp. 306–311.
- [22] Motoo, K., Arai, F., Fukuda, T., Matsubara, M., Kikuta, K., Yamaguchi, T. & Hirano, S. 2005, 'Touch sensor for micromanipulation with pipette using lead-free (K,Na)(Nb,Ta)O₃ piezoelectric ceramics', *Journal of Applied Physics*, vol. 98, no. 9, p. 094505.
- [23] Wich, T. & Fatikow, S. 2007, 'Assembly in the SEM', *Robotics Science and Systems Conference* - <http://www.me.cmu.edu/faculty1/sitti/RSS06/RSSWorkshop.htm>.
- [24] Wang, X., Ananthasuresh, G.K. & Ostrowski, J.P. 20 November 2001, 'Vision-based sensing of forces in elastic objects', *Sensors and Actuators A: Physical*, vol. 94, pp. 142–156(15).
- [25] Greminger, M. A. & Nelson, B. J. 2004, 'Vision-based force measurement', *IEEE Transactions on Pattern Analysis and Machine Intelligence*, vol. 26, no. 3, pp. 290–298.
- [26] Wich, T., Sievers, T. & Fatikow, S. 2006, 'Assembly inside a scanning electron microscope using electron beam induced deposition', *Proc. Int. Conf. on Intelligent Robots and Systems (IROS'06)*, Beijing, China, pp. 294–299.
- [27] Zhou, Q., Aurelian, A., Chang, B., del Corral, C. & Koivo, H. N. 2004, 'Micro-assembly system with controlled environment', *Journal of Micromechatronics*, vol. 2, no. 3-4, pp. 227–248.
- [28] Sievers, T. & Fatikow, S. 2005, 'Visual servoing of a mobile microrobot inside a scanning electron microscope', *Proc. Int. Conf. on Intelligent Robots and Systems (IROS'05)*, Edmonton, Canada, pp. 1682–1686.
- [29] Jähnisch, M., Hülsen, H., Sievers, T. & Fatikow, S. 2005, 'Control system of a nanohandling cell within a scanning electron microscope', *Proc. Int. Symposium on Intelligent Control (ISIC'05) / Mediterranean Conference on Control and Automation (MED'05)*, Limassol, Cyprus, pp. 964–969.
- [30] PiezoMotor AB Sweden, 2007, 'Homepage', online: <http://www.piezomotor.se/>.
- [31] Nascatec GmbH Germany, 2007, 'Homepage', online: <http://www.nascatec.de>.
- [32] Kortschack, A., Hänßler, O. C., Rass, C. & Fatikow, S. 2003, 'Driving principles of mobile microrobots for the micro- and nanohandling', *Proc. Int. Conf. on Intelligent Robots and Systems (IROS'03)*, Las Vegas, USA., pp. 1895–1900.
- [33] Kortschack, A. & Fatikow, S. 2004, 'Development of a mobile nanohandling robot', *Journal of Micromechatronics*, vol. 2, no. 3-4, pp. 249–269.
- [34] Kortschack, A., Shirinov, A., Trüper, T. & Fatikow, S. 2005, 'Development of mobile versatile nanohandling microrobots: design, driving principles, haptic control', *Robotica*, vol. 23, no. 4, pp. 419–434.
- [35] Carl Zeiss SMT AG Germany, 2007, 'Homepage', online: <http://www.smt.zeiss.com/>.
- [36] Point Electronic GmbH Germany, 2007, 'Homepage', <http://pointelectronic.de/>.
- [37] Sievers, T. & Fatikow, S. 2005, 'Pose estimation of mobile microrobots in a scanning electron microscope', *Proc. Int. Conference on Informatics in Control, Automation and Robotics (ICINCO'05)*, Barcelona, Spain, pp. 193–198.

- [38] Sievers, T. & Fatikow, S. 2006, 'Real-Time Object Tracking for the Robot-Based Nanohandling in a Scanning Electron Microscope', *Journal of Micromechatronics - Special Issue on Micro/Nanohandling*, vol. 3, no. 3-4, pp. 267–284(18).
- [39] Sievers, T. 2006, 'Global sensor feedback for automatic nanohandling inside a scanning electron microscope', *Proc. Virtual Int. Conference on Intelligent Production Machines and Systems*, pp. 289–294, <http://conference.iproms.org/>.
- [40] MicroE Systems MA USA, 2007, 'Homepage', online: <http://www.microesys.com/>.



<http://www.springer.com/978-1-84628-977-4>

Automated Nanohandling by Microrobots

Fatikow, S. (Ed.)

2008, XVI, 346 p., Hardcover

ISBN: 978-1-84628-977-4